Mechanics of the Human Hamstring Muscles during Sprinting

ANTHONY G. SCHACHE[1], TIM W. DORN[1], PETER D. BLANCH[2], NICHOLAS A. T. BROWN[3], and MARCUS G. PANDY[1]

[1]Department of Mechanical Engineering, University of Melbourne, Victoria, AUSTRALIA; [2]Department of Physical Therapies, Australian Institute of Sport, Belconnen ACT, AUSTRALIA; and [3]Department of Biomechanics and Performance Analysis, Australian Institute of Sport, Belconnen ACT, AUSTRALIA

ABSTRACT

SCHACHE, A. G., T. W. DORN, P.D. BLANCH, N. A. T. BROWN, and M. G. PANDY. Mechanics of the Human Hamstring Muscles during Sprinting. *Med. Sci. Sports Exerc.*, Vol. 44, No. 4, pp. 647–658, 2012. **Purpose**: An understanding of hamstring mechanics during sprinting is important for elucidating why these muscles are so vulnerable to acute strain-type injury. The purpose of this study was twofold: first, to quantify the biomechanical load (specifically, musculotendon strain, velocity, force, power, and work) experienced by the hamstrings across a full stride cycle; and second, to determine how these parameters differ for each hamstring muscle (i.e., semimembranosus (SM), semitendinosus (ST), biceps femoris long head (BF^{LH}), biceps femoris short head (BF^{SH})). **Methods**: Full-body kinematics and ground reaction force data were recorded simultaneously from seven subjects while sprinting on an indoor running track. Experimental data were integrated with a three-dimensional musculoskeletal computer model comprised of 12 body segments and 92 musculotendon structures. The model was used in conjunction with an optimization algorithm to calculate musculotendon strain, velocity, force, power, and work for the hamstrings. **Results**: SM, ST, and BF^{LH} all reached peak strain, produced peak force, and performed much negative work (energy absorption) during terminal swing. The biomechanical load differed for each hamstring muscle: BF^{LH} exhibited the largest peak strain, ST displayed the greatest lengthening velocity, and SM produced the highest peak force, absorbed and generated the most power, and performed the largest amount of positive and negative work. **Conclusions**: As peak musculotendon force and strain for BF^{LH}, ST, and SM occurred around the same time during terminal swing, it is suggested that this period in the stride cycle may be when the biarticular hamstrings are at greatest injury risk. On this basis, hamstring injury prevention or rehabilitation programs should preferentially target strengthening exercises that involve eccentric contractions performed with high loads at longer musculotendon lengths. **Key Words:** RUNNING BIOMECHANICS, MUSCLE FORCE, MUSCLE FUNCTION, MUSCLE INJURY, MUSCULOSKELETAL MODELING

Acute strain-type injuries to lower limb skeletal muscles have a high incidence rate in many popular sports, such as soccer (13) and rugby (15), and can create considerable cost in lost training and competition time. Of these injuries, the hamstring muscles are by far the most frequently involved (13,15). Although sports participation can involve a variety of skills that can potentially load the hamstrings (e.g., kicking, twisting, jumping), it has been reported that the majority of hamstring muscle strain-type injuries occur while the athlete is running at maximal or close to maximal speeds (4). A complete understanding of the biomechanical function of the hamstring muscles during sprinting is therefore required to aid in the development of rehabilitation and prevention strategies that are targeted to the mechanism of injury.

Most studies to date have measured electromyographic (EMG) activity and/or have applied an inverse dynamics approach to evaluate hamstring muscle function during sprinting. For example, studies involving recordings of EMG activity have found the hamstrings to be active from midswing until terminal stance (7,21,23,25,26,35,45). Some of these studies have reported peak activity to occur during terminal swing (21,26,45), whereas others have found it to occur during stance (23,25). Studies have also made inferences about hamstring muscle function during sprinting from

Address for correspondence: Anthony G. Schache, Ph.D., Department of Mechanical Engineering, University of Melbourne, Victoria 3010, Australia; E-mail: anthonys@unimelb.edu.au.
Submitted for publication June 2011.
Accepted for publication September 2011.

Supplemental digital content is available for this article. Direct URL citations appear in the printed text and are provided in the HTML and PDF versions of this article on the journal's Web site (www.acsm-msse.org).

0195-9131/12/4404-0647/0
MEDICINE & SCIENCE IN SPORTS & EXERCISE®

DOI: 10.1249/MSS.0b013e318236a3d2

net lower limb joint moments and powers calculated using standard inverse dynamics (32,35,43). Such studies have shown a hip extensor moment to be present from midswing until early stance, along with a knee flexor moment during terminal swing, implying that considerable load is likely imparted onto the hamstrings.

Although EMG- and/or inverse dynamics–based analyses have provided some important insights, the ability of these approaches to quantify the biomechanical load experienced by a given muscle during a functional motor task is limited in two main ways. First, the human musculoskeletal system is mechanically redundant. Many muscles cross each joint, and so a net joint moment can be satisfied by an infinite combination of muscle forces. Biarticular muscles such as the hamstrings span two joints—the hip and the knee—and so contribute to the net moments exerted about both joints simultaneously. It is therefore not possible to discern the actions of individual muscles from net joint moments alone (29). Second, EMG recordings primarily establish whether a muscle is active or not. Determining muscle force from EMG data is not a straightforward process, particularly for fast dynamic activities like sprinting. This is because many factors influence the relation that may exist between the EMG signal and the force developed by a muscle, including (but not limited to) muscle length, muscle fatigue, elastic properties of the musculotendon unit, contraction type, contraction velocity, as well as the level of contribution provided by synergistic muscles (12). Furthermore, the risk of crosstalk when recording EMG data from muscles that lie near each other can never be entirely avoided. One way to overcome these limitations is via advanced musculoskeletal modeling.

Models of the musculoskeletal system can be particularly advantageous for investigating the mechanics of a specific muscle group, such as the hamstrings (6,7,33–35,39,40,43,45). This is because musculoskeletal models have the capacity to estimate several additional and potentially significant parameters. For example, by including detailed anatomical information, such models allow musculotendon length to be estimated (35,40,43,45). This parameter is likely to be of particular relevance in the context of acute muscle strain-type injuries because animal-based experimental evidence exists demonstrating that the amount of musculotendon strain that occurs during repeated eccentric contractions is highly related to the severity of the subsequent muscle damage (28). Furthermore, it is possible to integrate musculoskeletal models with mathematical optimization routines to estimate additional parameters, such as musculotendon force, power, and work done, which are otherwise unmeasurable by noninvasive means (29). Musculoskeletal modeling is therefore a commonly used tool for studying the biomechanics of human movement, and it has proven to be a powerful method for advancing current understanding of muscle function (29,47).

Published research involving the application of musculoskeletal models to specifically evaluate hamstring muscle function during sprinting already exists (6,7,33–35,39,40,43,45). Some studies have focused on hamstring kinematics during sprinting and have found the peak length of the musculotendon unit to occur during terminal swing just before foot-strike (34,35,40,43,45). Peak length is approximately 10% greater than that assumed during an upright stance pose, and it does not seem to vary significantly as running is progressed from submaximal to maximal speeds (40). Other studies have estimated additional parameters such as hamstrings muscle force, power, and work done (6,7,33,39). These parameters, in contrast to musculotendon length, have all been shown to steadily increase with speed. For instance, an increase in running speed from 80% to maximum was associated with an increase in net hamstring muscle force and energy absorption during terminal swing of 1.4-fold and 1.9-fold, respectively (6). Unfortunately, however, studies to date that have quantified hamstrings muscle force, power, and work done during sprinting have collected data using a treadmill (6,7,39), evaluated the swing phase of the stride cycle only (6,39), obtained data for a single subject only (33,39), or modeled the hamstring muscle complex as a single unit (33). A more complete analysis of the biomechanical load experienced by the hamstrings during overground sprinting is therefore required.

In the present study, a three-dimensional (3D) musculoskeletal computer model was used in conjunction with subject-specific experimental data to study the mechanics of the hamstring muscles during human sprinting. The aim of the study was twofold: first, to quantify the biomechanical load (specifically, musculotendon strain, velocity, force, power, and work) experienced by the hamstrings across a full stride cycle during overground sprinting; and second, to determine how the biomechanical load differs for each individual hamstring muscle (i.e., semimembranosus (SM), semitendinosus (ST), biceps femoris long head (BF^{LH}), biceps femoris short head (BF^{SH}).

METHODS

Subjects. Seven subjects (five males and two females) volunteered to participate in this study. Subjects had a mean ± SD age of 26.6 ± 8.3 yr, a mean ± SD height of 177.9 ± 5.6 cm, and a mean ± SD body mass of 74.4 ± 8.2 kg. All subjects were experienced sprinters and, at the time of testing, were not suffering from any musculoskeletal injury likely to adversely affect their sprinting mechanics. Subjects were not specifically excluded if they had a history of an acute hamstring muscle strain-type injury. Four of the subjects had never suffered a hamstring injury, whereas two subjects had a history of bilateral hamstring injuries and one subject had a history of a unilateral hamstring injury. The study was approved by the Human Research Ethics Committee at The University of Melbourne and The Australian Institute of Sport, and all participants gave their written informed consent before testing.

Experimental data collection. Data collection took place on an indoor 110-m synthetic running track in the

Biomechanics Laboratory at the Australian Institute of Sport. Kinematic data were recorded using a 3D motion analysis system (VICON; Oxford Metrics Ltd., Oxford, United Kingdom) with 22 cameras sampling at 250 Hz. The measurement volume had a length, width, and height of 15, 1.3, and 2.2 m, respectively, and was situated approximately 80 m along the 110-m running track, providing ample distance for acceleration and deceleration. Ground reaction force (GRF) data were recorded via eight large (900 × 600 mm) force plates (Kistler Instrument Corp., Amherst, NY), sampling at 1500 Hz. Force plates were embedded in the laboratory floor and were covered with individual pieces of the synthetic running track to disguise their actual location. The force plates were embedded immediately adjacent to each other (thereby expanding a total length of 7.2 m) and were situated in the center of the measurement volume. GRF data were low-pass filtered using a fourth-order Butterworth filter with a cutoff frequency of 60 Hz before data processing. Hamstring EMG activity was recorded using a telemetered system (Noraxon Telemyo 2400 G2; Noraxon USA, Inc., Scottsdale, AZ) at a sampling rate of 1500 Hz. To facilitate the precise determination of onset and offset times, a Taeger–Kaiser energy operator was applied to the raw EMG signal to increase the detection accuracy of the EMG burst boundaries (27,36).

For each subject, one lower limb was designated as the side to be tested (or lower limb of interest) for purposes of the study. This lower limb was the left side for four subjects and the right side for three subjects. Subjects wore athletic shorts and running sandals (Nike Straprunner IV, Beaverton, OR) for testing. Running sandals were used rather than conventional running shoes to allow exposure of the foot for marker placement. This decision was based on studies demonstrating that shoe-mounted markers do not seem capable of providing a true reflection of underlying foot motion (31,37). Standard anthropometric parameters (i.e., height and body mass) were initially measured. Bipolar silver/silver chloride surface electrodes with a 10-mm-diameter contact area and a fixed interelectrode distance of 20 mm (Nicolet Biomedical, Memphis, TN) were mounted on the posterior aspect of the thigh in accordance with SENIAM recommendations (20). For the medial hamstrings, surface electrodes were positioned on the midpoint of a line connecting the ischial tuberosity and medial tibial epicondyle, whereas for the lateral hamstrings, surface electrodes were positioned on the midpoint of a line connecting the ischial tuberosity and the lateral tibial epicondyle. A ground electrode (3M Health Care, St. Paul, MN) was placed over the proximal end of the anteromedial shaft of the tibia. A total of 50 small (14 mm) reflective markers were mounted at specific anatomical locations on each subject's whole body, and a static trial was captured with the subject assuming a neutral pose. After the static trial, subjects were provided with sufficient time to warm-up (repeated strides of increasing speed) after which they performed maximal sprinting. Sprinting speed was measured using timing gates (Speedlight Telemetry Timing; Swift Performance Equipment, Queensland, Australia), which were located 20 m apart at either end of the measurement volume. A single representative trial containing valid force plate contacts for a complete stride cycle for the designated lower limb of interest (i.e., initial foot-strike and foot-off for the ipsilateral limb, followed by foot-strike and foot-off for the contralateral limb, followed by another foot-strike and foot-off for the ipsilateral limb) was recorded and analyzed for each subject.

Musculoskeletal model. A generic musculoskeletal model was accessed from OpenSim (10). The skeleton was represented by a 3D 12-segment, 31-degree-of-freedom linkage (Fig. 1A). The head and torso were lumped together and represented as a single rigid body (i.e., the trunk), which articulated with the pelvis via a ball-and-socket joint located approximately at the third lumbar vertebra (2,3). For the lower limbs, each hip was modeled as a ball-and-socket joint, each knee as a translating hinge joint (44), and each ankle complex as two nonintersecting pure hinge joints (11). All degrees-of-freedom for the trunk-to-pelvis and lower limb joints were actuated by a total of 92 musculotendon structures (Fig. 1B), each represented as a Hill-type muscle in series with the tendon (46) (Fig. 1C). Muscle lines of action in the musculoskeletal model were identical with those of Hamner et al. (17). For the upper limb, each shoulder was modeled as a ball-and-socket joint and each elbow as two nonintersecting hinge joints (22). The upper limb joints were actuated by 10 pure torque motors to model the dynamics of arm swing.

Subject-specific musculoskeletal models were then generated in OpenSim (10) by scaling the generic model according to individual subject anthropometry. Specifically, individual segment scale factors were calculated using the ratio of the distances between two markers on the segment during the static standing calibration trial and the distances between the same two markers on the musculoskeletal model. These scale factors were then used to scale segment lengths, segment inertial properties, and muscle attachment points (10).

Joint kinematics across the entire stride cycle were computed by performing an inverse kinematic analysis, which minimized the sum of the squared differences between the positions of virtual markers on the musculoskeletal model and those placed on the subject. Resulting joint kinematics were passed into a residual reduction algorithm (10). This algorithm refined the estimates obtained from inverse kinematics to improve their dynamic consistency with the recorded GRF data. All lower limb joint moments were computed via an inverse dynamics approach. A static optimization algorithm (3) was used to calculate individual musculotendon forces taking into account the prescribed force–length–velocity properties for each musculotendon structure in the model (Table 1 outlines the values used for each of the hamstring muscles). Specifically, the muscular load sharing problem was solved for each time point in the stride cycle by minimizing a performance criterion as well as satisfying the equality of the sum of individual muscular

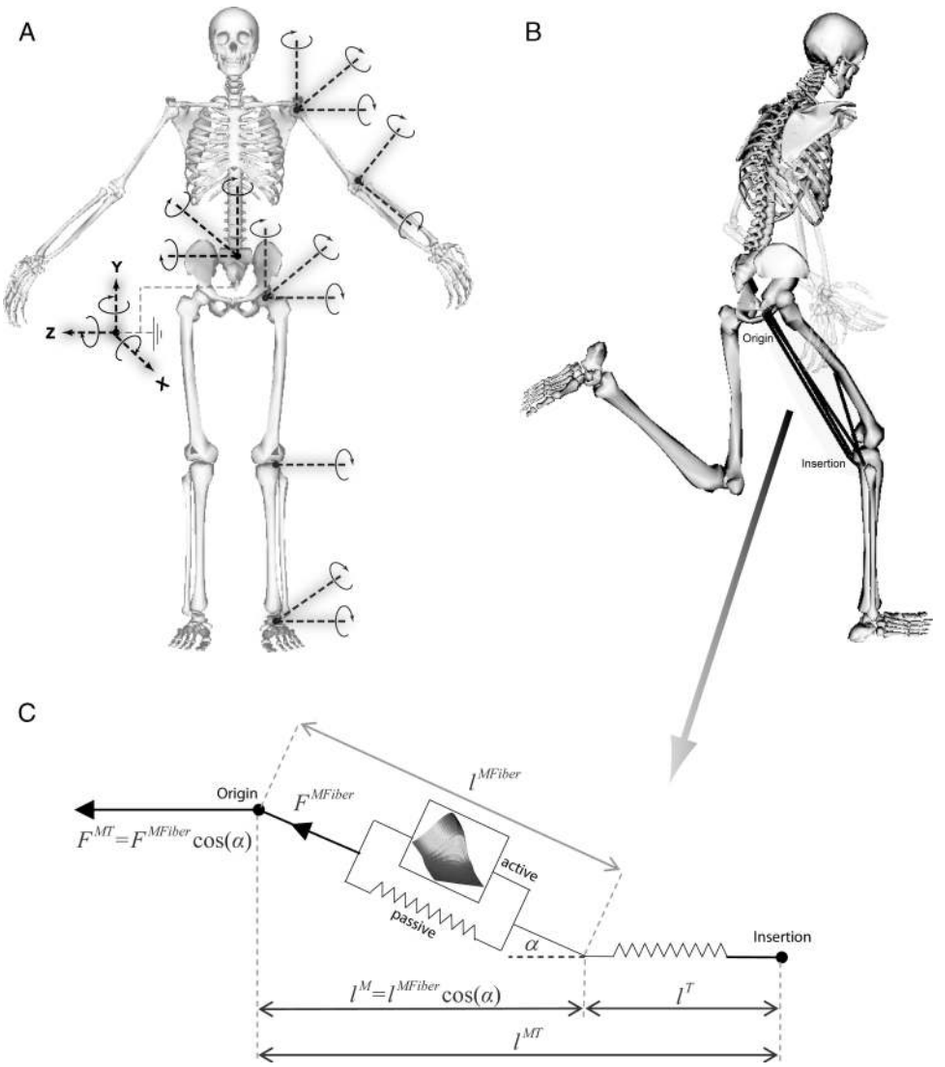

FIGURE 1—Three-dimensional musculoskeletal computer model used in this study. A, The skeleton was represented as a multibody linkage containing 11 degrees of freedom. B, The lower limb joints and trunk were driven by 92 musculotendon actuators, whereas the upper limb joints were driven by 10 ideal torque actuators. For clarity, only the four hamstring muscles for the right lower limb are shown in the figure. C, Each musculotendon actuator was represented as a Hill-type physiological muscle in series with tendon. Musculotendon length (l^{MT}) was equal to the sum of the muscle (l^{M}) and tendon lengths (l^{T}), where l^{M} was defined as the projection of the muscle fiber length (l^{MFiber}) in the direction of the tendon. Muscle pennation angle is represented by the symbol α. Musculotendon force (F^{MT}) was defined as the projection of the muscle fiber force (F^{MFiber}) in the direction of the tendon.

moments (i.e., force multiplied by moment arm for each muscle) to the joint moments obtained from the inverse dynamics analysis. The performance criterion applied in the present study was to minimize the sum of the square of muscle activations (3). This particular performance criterion was chosen for three main reasons. First, this criterion has

TABLE 1. Musculotendon force–length–velocity properties for each of the individual hamstrings.

Property	SM	ST	BF^{LH}	BF^{SH}
Tendon slack length, $l_{s_T}^{T}$ (m)	0.3440	0.2755	0.3350	0.1517
Tendon compliance, ε_0^{T}	0.033	0.033	0.033	0.033
Optimal muscle fiber length, l_0^{M} (m)	0.0800	0.2010	0.1000	0.1103
Maximum shortening velocity, V_{max} ($m \cdot s^{-1}$)	1.600	4.020	2.000	2.206
Maximum isometric force, F_0^{M} (N)	3864	1230	2688	2412
Optimal muscle fiber pennation angle, α_0 (°)	15.0	13.0	11.6	12.3

$l_{s_T}^{T}$ Based on data reported by Delp et al. (11).
ε_0^{T} Recommended value reported by Zajac (46).
l_0^{M} Based on data reported by Wickiewicz et al. (42) and Ward et al. (41).
V_{max} Calculated as $20 \times l_0^{M}$.
α_0 Based on data reported by Ward et al. (41).

been used by previous researchers to estimate lower limb muscle forces during walking (2,3,9), running (16,29), and sprinting (6,7,39). Second, it has been demonstrated that the number of active muscles computed is greater for nonlinear compared with linear criteria (30). Third, this criterion has been previously shown to predict lower limb muscle forces that have similar time histories to experimental measurements of EMG activity during walking (2) and running (16,29).

The hamstring muscle complex was represented by three biarticular structures (SM, ST, and BF^{LH}) and one uniarticular structure (BF^{SH}). For each individual hamstring muscle, the primary outcome measures of interest were musculotendon strain, velocity, force, power, and work. These parameters were calculated as follows. Musculotendon length (l^{MT}) was equal to the sum of the muscle (l^{M}) and tendon lengths (l^{T}), where l^{M} was defined as the projection of the muscle fiber length (l^{MFiber}) in the direction of the tendon (Fig. 1C). Musculotendon strain was calculated as the change in l^{MT} from that assumed for the static standing calibration trial (expressed as a percentage increase or decrease). Musculotendon velocity (V^{MT}) was represented as the first derivative of length with respect to time, that is, $V^{MT} = dl^{MT}/dt$. Musculotendon force (F^{MT}) was defined as the projection of the muscle fiber force (F^{MFiber}) in the direction of the tendon (Fig. 1C). Musculotendon power (P^{MT}) was calculated as the product of musculotendon force and velocity, that is, $P^{MT} = F^{MT}V^{MT}$. Work was found by integrating power with respect to time; that is, by calculating the area under the power–time curve. Positive work represented power generation (concentric contraction) and negative work represented power absorption (eccentric contraction).

Data analysis. Data were analyzed for the designated lower limb of interest for each subject (i.e., the left side for four subjects and the right side for three subjects). To evaluate the similarity between the moments derived from inverse dynamics and those produced by the muscles, the RMS of the difference between the two joint moments was calculated for each subject and then averaged across all subjects. This process was repeated for all six lower limb joint moments. The primary outcome measures of interest (musculotendon length, velocity, force, and power) were normalized as a percentage of the full stride cycle (0%–100%) from ipsilateral foot-off to the following ipsilateral foot-off for each individual hamstring muscle. Foot-off (rather than foot-strike) was used to define the start and finish of the stride cycle because this is the least critical period in terms of hamstring muscle function. Once time normalized for each subject, data were then averaged across subjects to generate mean (±1 SD) plots for each individual hamstring muscle. Hamstring EMG activity onset and offset times across the stride cycle were visually determined using the Taeger–Kaiser energy operator–filtered signal (36). In addition to generating plots, discrete variables were extracted from the data set. Various maxima and minima points that were readily identifiable on the musculotendon length, velocity, force, and power profiles for each individual hamstring muscle were selected. The total amount of positive and negative work done during swing, stance, and over the full stride cycle were also calculated. Group mean (±1 SD) values for each of the variables for each individual hamstring muscle were calculated.

RESULTS

The average sprinting speed for the cohort was 8.95 ± 0.70 $m \cdot s^{-1}$ (range = 7.90–9.72 $m \cdot s^{-1}$). Overall, there was close agreement between the joint moments derived from inverse dynamics and those derived from the computed muscle forces (Fig. 2). The average RMS of the difference between the two joint moments was found to be less than

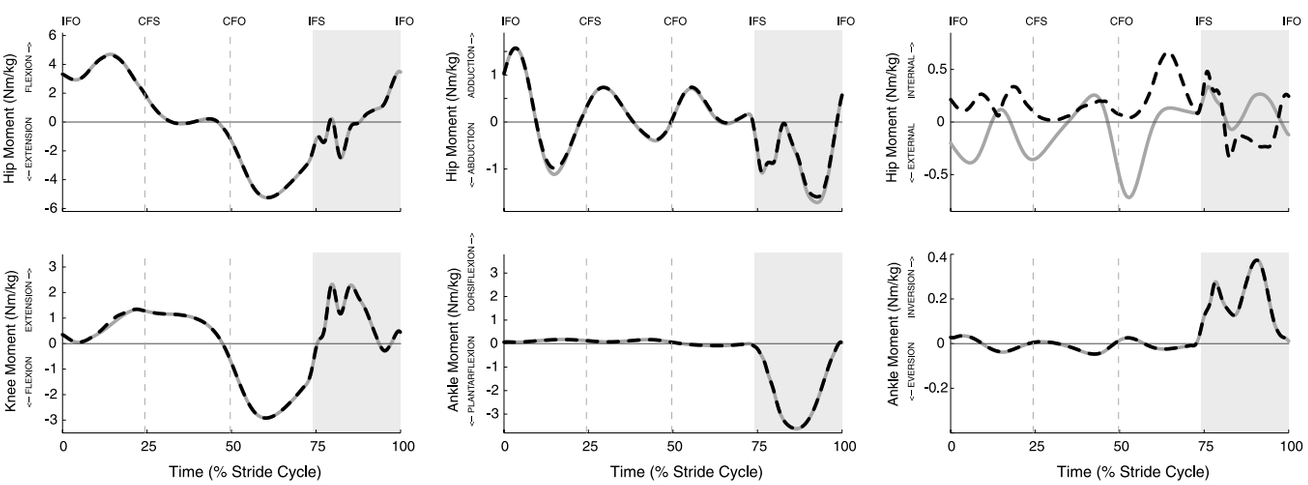

FIGURE 2—Group mean lower limb internal joint moments derived from inverse dynamics (*solid gray line*) and those derived from the computed muscle forces (*dashed black line*) across a full stride cycle. The *light gray shading* in each panel indicates the stance phase of the stride cycle. IFO, ipsilateral foot-off; CFS, contralateral foot-strike; CFO, contralateral foot-off; IFS, ipsilateral foot-strike.

0.05 N·m·kg^{-1}, with the exception of the transverse plane hip moment (internal/external rotation) where the average RMS of the difference was 0.45 N·m·kg^{-1}. The evident discrepancy between the muscle-computed and the inverse dynamics–computed transverse plane hip moment was most likely attributable to errors in the experimental data (e.g., soft tissue artifact). However, this discrepancy was not considered to be of any major consequence for predicting hamstring muscle forces because (a) the amplitude of the transverse plane hip moment was quite small relative to the sagittal plane hip and knee moments and (b) the biarticular hamstrings are not primary axial rotators of the hip joint. The static optimization analysis was therefore deemed successful in generating a set of muscle forces that could adequately recover the joint moments derived from inverse dynamics.

The biarticular hamstring muscles lengthened from early swing (~20% of the stride cycle) until terminal swing (~60% of the stride cycle), after which they shortened and continued to do so for the duration of stance (Fig. 3, row 1). Peak musculotendon strain for BF^{LH} during sprinting was, on average, 12.0 ± 2.6%, which exceeded the peak values of musculotendon strain for SM and ST by 2.2% and 3.3%, respectively (Table 2). Furthermore, the time of peak musculotendon strain for BF^{LH} preceded that for SM and ST by approximately 1.5% of the stride cycle.

During early swing (0%–20% of the stride cycle), the rate at which the hamstring muscles shortened increased initially and then reduced (Fig. 3, row 2). The average peak musculotendon shortening velocity at this time ranged from 0.74 ± 0.09 m·s^{-1} for BF^{SH} to 1.04 ± 0.12 m·s^{-1} for ST (Table 2). During the middle stages of swing (20%–60% of the stride

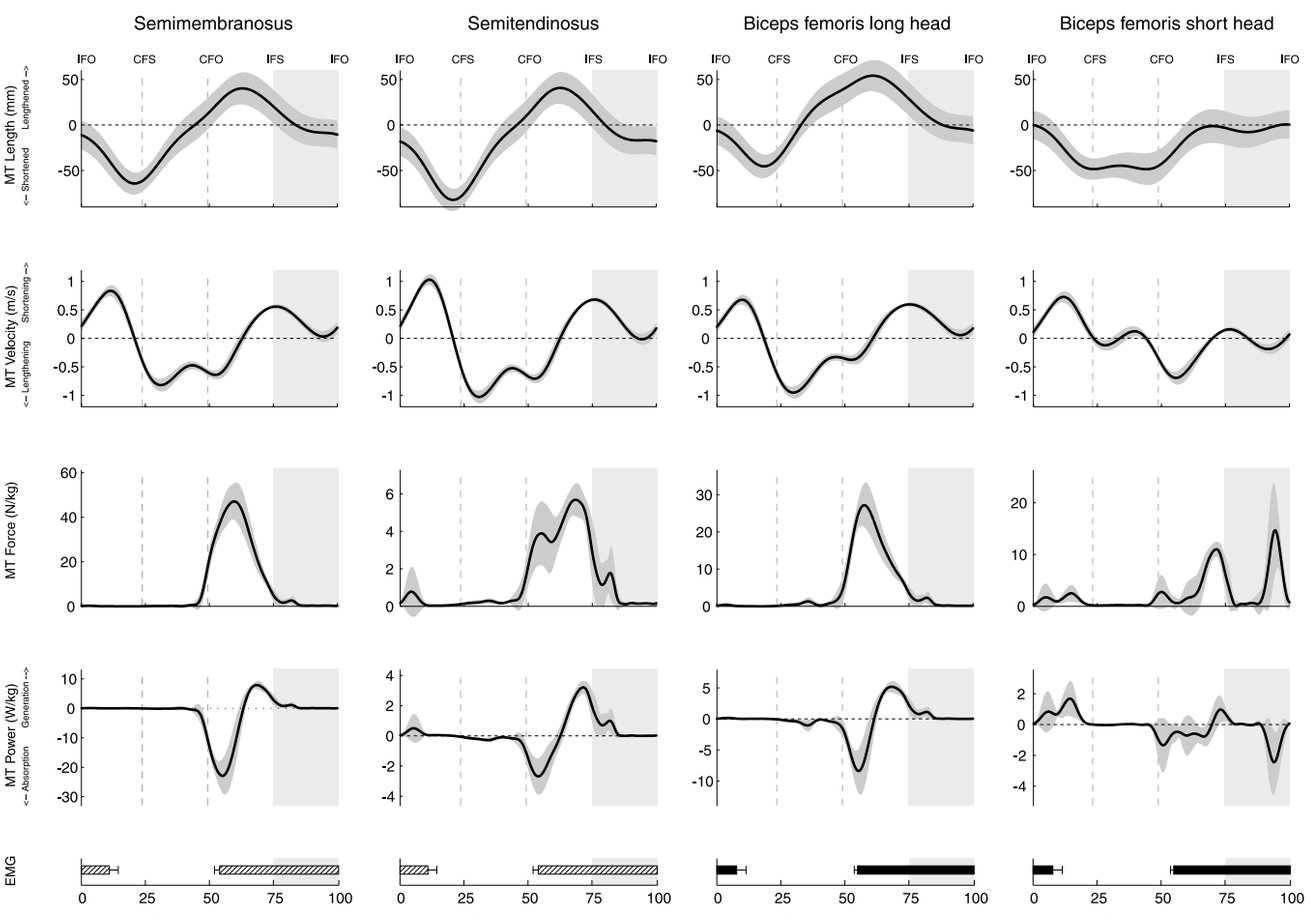

FIGURE 3—Musculotendon (MT) length (*top row*), velocity (*second row*), force (*third row*), and power (*fourth row*) for each hamstring muscle across a full stride cycle. Each panel displays the group mean (*solid black line*) ± 1 SD (*gray band*). The group mean ± 1 SD onset and offset times as a percent of the stride cycle for the medial (*horizontal bar filled with black diagonal lines*) and lateral (*solid black horizontal bar*) hamstrings EMG data are displayed in the *bottom panels*. It was assumed that the surface electrodes mounted over the medial hamstrings recorded the combined EMG activity from semimembranosus and semitendinosus, whereas the surface electrodes mounted over the lateral hamstrings recorded the combined EMG activity from biceps femoris long head and short head. Note therefore that the onset and offset times for the medial hamstrings EMG included in the columns for semimembranosus and semitendinosus represent the same data. Similarly, the onset and offset times for the lateral hamstrings EMG included in the columns for biceps femoris long head and short head represent the same data. The *light gray shading* in each panel indicates the stance phase of the stride cycle. IFO, ipsilateral foot-off; CFS, contralateral foot-strike; CFO, contralateral foot-off; IFS, ipsilateral foot-strike.

TABLE 2. Mean ± 1 SD values for the various discrete parameters extracted from the data set (i.e., musculotendon strain, velocity, force, power, and work for each of the hamstring muscles).

	SM	ST	BF^{LH}	BF^{SH}
Strain				
Peak strain (% change from static pose)	9.84 ± 1.15	8.73 ± 1.31	11.98 ± 2.63	—
Time of peak strain (% stride cycle)	62.76 ± 1.56	62.37 ± 1.53	60.87 ± 1.71	—
Velocity				
First peak shortening velocity ($m \cdot s^{-1}$)	0.84 ± 0.10	1.04 ± 0.12	0.69 ± 0.08	0.74 ± 0.09
Time first peak shortening velocity (% stride cycle)	11.36 ± 0.99	11.34 ± 1.00	9.80 ± 1.03	11.70 ± 1.15
Peak lengthening velocity ($m \cdot s^{-1}$)	−0.84 ± 0.08	−1.04 ± 0.13	−0.96 ± 0.12	−0.71 ± 0.05
Time peak lengthening velocity (% stride cycle)	34.20 ± 8.17	33.97 ± 8.31	29.80 ± 0.70	55.80 ± 1.39
Second peak shortening velocity ($m \cdot s^{-1}$)	0.56 ± 0.04	0.69 ± 0.06	0.60 ± 0.04	0.16 ± 0.07
Time second peak shortening velocity (% stride cycle)	75.97 ± 1.21	75.79 ± 1.18	75.10 ± 1.73	76.74 ± 1.35
Force				
Peak force during swing ($N \cdot kg^{-1}$)	46.81 ± 6.25	5.49 ± 0.78	26.35 ± 5.15	10.36 ± 1.47
Time peak force during swing (% stride cycle)	59.34 ± 2.16	66.94 ± 5.32	57.40 ± 1.03	72.00 ± 1.97
Peak force during stance ($N \cdot kg^{-1}$)	6.48 ± 1.63	3.64 ± 0.73	4.61 ± 0.99	14.78 ± 7.99
Time peak force during stance (% stride cycle)	74.47 ± 1.31	74.47 ± 1.31	74.47 ± 1.31	91.31 ± 7.60
Power				
Peak power absorption ($W \cdot kg^{-1}$)	−22.39 ± 5.40	−2.70 ± 1.01	−8.31 ± 3.34	−2.60 ± 1.90
Time peak power absorption (% stride cycle)	55.07 ± 1.40	54.99 ± 2.78	55.11 ± 1.24	85.96 ± 13.92
Peak power generation ($W \cdot kg^{-1}$)	7.66 ± 1.14	3.13 ± 0.46	5.00 ± 0.84	2.05 ± 1.04
Time peak power generation (% stride cycle)	68.07 ± 1.13	72.11 ± 1.99	67.66 ± 1.16	21.21 ± 23.06
Work				
Negative work done during swing ($J \cdot kg^{-1}$)	−1.06 ± 0.25	−0.13 ± 0.05	−0.34 ± 0.12	−0.07 ± 0.07
Positive work done during swing ($J \cdot kg^{-1}$)	0.31 ± 0.06	0.13 ± 0.04	0.24 ± 0.04	0.09 ± 0.03
Negative work done during stance ($J \cdot kg^{-1}$)	0.00 ± 0.00	0.00 ± 0.00	0.00 ± 0.00	−0.06 ± 0.05
Positive work done during stance ($J \cdot kg^{-1}$)	0.06 ± 0.02	0.04 ± 0.02	0.05 ± 0.02	0.01 ± 0.00
Total negative work done ($J \cdot kg^{-1}$)	−1.06 ± 0.25	−0.13 ± 0.05	−0.34 ± 0.12	−0.13 ± 0.10
Total positive work done ($J \cdot kg^{-1}$)	0.37 ± 0.07	0.17 ± 0.04	0.29 ± 0.05	0.10 ± 0.03

cycle), the musculotendon lengthening velocity of the hamstrings showed a characteristic biphasic pattern (Fig. 3, row 2). The average peak musculotendon lengthening velocity at this time ranged from -0.71 ± 0.05 $m \cdot s^{-1}$ for BF^{SH} to -1.04 ± 0.13 $m \cdot s^{-1}$ for ST (Table 2). For BF^{LH}, the first peak in the musculotendon lengthening velocity during swing was always larger than the second, whereas the opposite was true for BF^{SH}. For SM and ST, the two peaks in the musculotendon lengthening velocity during swing were closer in magnitude, with some subjects having a larger first peak, whereas others displayed a larger second peak. During terminal swing (60%–75% of the stride cycle), the musculotendon shortening velocity of the hamstring muscles increased once more (Fig. 3, row 2). The average peak musculotendon shortening velocity at this time occurred just after foot-strike and ranged in magnitude from 0.16 ± 0.07 $m \cdot s^{-1}$ for BF^{SH} to 0.69 ± 0.06 $m \cdot s^{-1}$ for ST (Table 2). The musculotendon shortening velocity of the hamstrings then decreased during the first half of stance. Whereas a musculotendon lengthening velocity occurred for BF^{SH} during midstance for all subjects, such was not the case for the biarticular hamstring muscles. A musculotendon lengthening velocity during midstance was displayed by only three subjects for ST and by only two subjects for BF^{LH} and SM.

The static optimization analysis predicted that SM, ST, and BF^{LH} produced force during terminal swing and early stance, whereas BF^{SH} produced force during terminal swing and the second half of stance (Fig. 3, row 3). Overall, there was reasonable agreement between the time during the stride cycle when the hamstring muscles were predicted to develop force and the time when the hamstring muscles were found to display EMG activity (Fig. 3, row 3 vs row 5). Average peak musculotendon force ranged from 5.49 ± 0.78 $N \cdot kg^{-1}$ for ST to 46.81 ± 6.25 $N \cdot kg^{-1}$ for SM (Table 2). In comparison to stance, peak musculotendon force produced during swing was increased by 7.2-fold, 1.5-fold, and 5.7-fold for SM, ST, and BF^{LH}, respectively, whereas it was decreased by 0.7-fold for BF^{SH}.

All hamstring muscles underwent a period of power absorption followed by a period of power generation during terminal swing (Fig. 3, row 4). The average peak musculotendon power absorption during terminal swing ranged from -2.60 ± 1.90 $W \cdot kg^{-1}$ for BF^{SH} to -22.39 ± 5.40 $W \cdot kg^{-1}$ for SM, whereas the average peak musculotendon power generation during terminal swing ranged from 1.12 ± 0.69 $W \cdot kg^{-1}$ for BF^{SH} to 7.66 ± 1.14 $W \cdot kg^{-1}$ for SM (Table 2). BF^{SH} also underwent a period of musculotendon power absorption during terminal stance (average magnitude of -2.47 ± 2.01 $W \cdot kg^{-1}$) and a period of musculotendon power generation during early swing (average magnitude of 1.90 ± 1.06 $W \cdot kg^{-1}$), which were likely a result of the optimization algorithm preferentially distributing load onto the BF^{SH} to control knee extension in late stance and then facilitate rapid knee flexion during early swing.

The biarticular hamstrings performed negative work only during terminal swing, whereas BF^{SH} performed a small amount of negative work during both terminal swing and terminal stance (Table 2). All of the hamstring muscles performed more positive work during swing than during stance. The average total amount of negative work done ranged from -0.13 ± 0.05 $J \cdot kg^{-1}$ for ST to -1.06 ± 0.25 $J \cdot kg^{-1}$ for SM, whereas the average total amount of positive work done ranged from 0.10 ± 0.03 $J \cdot kg^{-1}$ for BF^{SH} to 0.37 ± 0.07 $J \cdot kg^{-1}$ for SM. Semitendinosus was the only hamstring muscle not

found to perform more negative work than positive work. In comparison to the total amount of positive work, the total amount of negative work was decreased 0.76-fold for ST and increased by 2.86-fold for SM.

DISCUSSION

The purposes of the present study were to quantify the biomechanical load (i.e., musculotendon strain, velocity, force, power, and work) experienced by the hamstrings across a full stride cycle during overground sprinting and to compare the biomechanical load across the four hamstring muscles (i.e., SM, ST, BF^{LH}, and BF^{SH}). The main outcomes can be summarized as follows. First, the biarticular hamstrings undergo a stretch–shortening cycle during sprinting, with the lengthening phase occurring during terminal swing and shortening phase commencing just before footstrike and continuing throughout stance. The timing of this stretch–shortening cycle corresponds with the period of hamstring EMG activity as measured in this study (Fig. 3, row 5) and in many previous studies (7,21,23,25,26,35,45). Second, the biomechanical load on the biarticular hamstring muscles was found to be greatest during terminal swing. At this time in the stride cycle, ST, SM, and BF^{LH} all reached peak musculotendon strain, produced peak musculotendon force, and performed much negative work. Third, when comparing the various hamstring muscles, the following results were found: (i) BF^{LH} had the largest peak musculotendon strain (12.0% increase in length from upright stance position), (ii) ST displayed the greatest musculotendon lengthening velocity, and (iii) SM produced the highest musculotendon force, absorbed and generated the most musculotendon power, and performed the largest amount of positive and negative work. These outcomes have implications for improving existing understanding of the pathomechanics of sprinting-related hamstring muscle strain-type injuries.

When comparing data from the present study with that from previous studies, the majority of the observed discrepancies are most likely attributable to the combined effect of three main factors. First, differences in the procedures used to record experimental data. In particular, several prior studies have measured data while sprinting on a treadmill (6,7,39), whereas data from the present study as well as those from Schache et al. (33) were measured while sprinting overground. Frishberg (14) compared treadmill and overground sprinting at 9.2 $m \cdot s^{-1}$ for five male athletes and found several trunk and lower limb kinematic parameters to be different between the two conditions. Second, differences in the computational approach adopted to estimate muscle forces. Thelen et al. (39) and Chumanov et al. (6,7) used a forward dynamics simulation approach (38), whereas Schache et al. (33) and the present study used an inverse dynamics–based static optimization approach (3). All studies have applied the same general performance criterion (i.e., minimization of the sum of the square of muscle activations [3]). However, whereas most studies have not imposed additional constraints on when, in the stride cycle, muscle activations can be predicted to occur, Chumanov et al. (7) explicitly constrained the hamstring and rectus femoris muscles to be inactive for a brief period during terminal stance and early swing. Third, variability in the maximum sprinting speeds investigated may explain, to some degree, discrepancies in reported results. The average sprinting speed in the present study was 9.0 $m \cdot s^{-1}$, whereas Schache et al. (33) recorded data at 7.4 $m \cdot s^{-1}$ and Chumanov et al. (7) used average maximum speeds of 8.0 and 7.1 $m \cdot s^{-1}$ for males and females, respectively. It is therefore possible that the larger hamstrings muscle forces in the present study compared with those in Schache et al. (33) and Chumanov et al. (7) are at least partially attributable to differences in test speeds. However, other studies (e.g., Thelen et al. [39] and Chumanov et al. [6]) involved maximum sprinting speeds that were

TABLE 3. Quantitative data for musculotendon force and work obtained from the present study compared to previous studies.

	V_{max} ($m \cdot s^{-1}$)	SM	ST	BF^{LH}	BF^{SH}	NET
Peak stance MT force ($N \cdot kg^{-1}$)						
Schache et al. (33)	7.5 ± 0.1	—	—	—	—	31.9 ± 11.4
Chumanov et al. (7)	7.1 and 8.0[a]	12.1 ± 2.4	6.2 ± 2.2	11.6 ± 1.9	—	—
Present study	9.0 ± 0.7	6.5 ± 1.6	3.6 ± 0.7	4.6 ± 1.0	14.8 ± 8.0	—
Peak swing MT force ($N \cdot kg^{-1}$)						
Thelen et al. (39)	9.3	—	—	17.6	—	—
Chumanov et al. (6)	8.2 ± 0.8 and 9.1 ± 0.6[b]	27.9 ± 7.6	7.9 ± 1.8	21.4 ± 5.4	—	52.0 ± 13.4
Schache et al. (33)	7.5 ± 0.1	—	—	—	—	46.5 ± 4.3
Chumanov et al. (7)	7.1 and 8.0[a]	23.9 ± 3.5	5.9 ± 1.9	13.2 ± 1.5	—	—
Present study	9.0 ± 0.7	46.8 ± 6.3	5.5 ± 0.8	26.4 ± 5.2	10.4 ± 1.5	—
Positive MT work ($J \cdot kg^{-1}$)						
Chumanov et al. (7)	7.1 and 8.0[a]	0.5 ± 0.1	0.3 ± 0.0	0.4 ± 0.1	—	—
Present study	9.0 ± 0.7	0.4 ± 0.1	0.2 ± 0.0	0.3 ± 0.1	0.1 ± 0.0	—
Negative MT work ($J \cdot kg^{-1}$)						
Chumanov et al. (6)	8.2 ± 0.8 and 9.1 ± 0.6[b]	1.0 ± 0.4	0.4 ± 0.2	0.8 ± 0.3	—	2.6 ± 1.0
Schache et al. (33)	7.5 ± 0.1	—	—	—	—	0.7 ± 0.1
Chumanov et al. (7)	7.1 and 8.0[a]	0.7 ± 0.1	0.4 ± 0.1	0.5 ± 0.1	—	—
Present study	9.0 ± 0.7	1.1 ± 0.3	0.1 ± 0.1	0.3 ± 0.1	0.1 ± 0.1	—

— Data not reported.
[a] Average maximum sprinting speed for females (n = 3) and males (n = 12), respectively (SD not reported).
[b] Average maximum sprinting speed for females (n = 5) and males (n = 14), respectively.
V_{max} average maximum sprinting speed.

similar in magnitude to the present study; hence, contrasting results in this instance cannot be explained on the basis of test speeds alone.

Despite the methodological differences among studies conducted to date, there is remarkable qualitative consistency in the reported findings. All studies have found the biarticular hamstrings to be subjected to large loads during the terminal swing phase of sprinting (6,7,33,39), with such loads exceeding those during stance (7,33). Furthermore, when comparing the various hamstrings, it has been found that BF^{LH} experiences the greatest musculotendon strain with respect to upright stance (6,7,34,40) and develops its peak musculotendon force slightly earlier in swing (6), whereas SM generates the largest peak musculotendon force and performs the greatest amount of work (6,7). These findings are all in agreement with the main outcomes from the present study. A quantitative comparison of results obtained from the various studies is given in Table 3. In some instances, data are reasonably similar; for example, the negative work done by SM during sprinting. However, for other parameters such as peak stance musculotendon force, data from the present study differ from equivalent data presented by Chumanov et al. (7) (see below).

Musculoskeletal modeling is the only practicable method for determining quantities such as muscle force, power, and work done under *in vivo* conditions (29). There is much evidence in the literature to show that computer-based models of the musculoskeletal system accurately predict biomechanical behavior. For instance, studies have compared model-derived estimates of hip- and knee-joint contact forces against simultaneously recorded *in vivo* data from instrumented (strain-gauged) joint implants for common activities of daily living, including walking (19,24) and stair climbing (19). These studies presented calculated joint contact forces that can be considered to be in good agreement with those directly measured from the instrumented joint implants. Although generating accurate estimates of joint contact forces is a necessary, but not sufficient, condition for concluding that the corresponding lower limb muscle forces are also accurate, confidence in model-derived estimates can be further increased by qualitatively comparing patterns of muscle forces with measured EMG data. In this regard, several studies have demonstrated that an inverse dynamics–based static optimization approach, as was used in the present study, is capable of producing lower limb muscle forces that have similar time histories to experimental measurements of EMG data for walking at the preferred speed (3) and running (16,29).

Unfortunately, as quantities such as muscle force, power, and work done cannot be measured *in vivo* by noninvasive means, it is not possible to directly validate estimates of hamstrings biomechanical load obtained in the present study. However, there are numerous factors that provide indirect evidence to indicate that the results from this study are reasonable. First, inverse dynamics–based joint moments in the present study are qualitatively and quantitatively consistent with equivalent data reported in the literature (1,32). Second, the estimation of large biomechanical loads on the biarticular hamstring muscles during the terminal swing phase of sprinting is in agreement with EMG studies that have reported peak activity of the medial and lateral hamstrings to occur during terminal swing (21,26,45). Third, sagittal plane moment arms for each of the hamstring muscles in the model plotted against hip- and knee-joint angle are consistent with experimental data from studies that have directly measured hamstrings moment arms using cadaveric specimens (see Figures, Supplemental Digital Contents 1 and 2, Sagittal plane moment arms at the hip and knee joint for each of the hamstring muscles in the model compared with available experimental data from studies that have directly measured hamstrings moment arms using cadaveric specimens; https://links.lww.com/MSS/A122, https://links.lww.com/MSS/A123). Finally, the estimated distribution of musculotendon force across the various hamstring muscles is consistent with their force-generating capacity based on muscle architecture. The distribution of musculotendon force across the hamstring muscles was primarily determined by the maximum isometric force (F_0^M) attributed to each muscle in the model. A given muscle's F_0^M is proportional to its physiological cross-sectional area (PCSA), which is a measure of the number of parallel muscle fibers acting within a muscle. Muscles with a larger PCSA have a greater force-generating capacity (41,42). Studies have used cadavers to directly calculate PCSA for the various hamstring muscles (41,42). Ward et al. (41) and Wickiewicz et al. (42) reported PCSA to range from 16.9 to 18.4 cm^2 and 4.8 to 5.4 cm^2 for SM and ST, respectively. Ward et al. (41) measured a PCSA of 11.3 cm^2 and 5.1 cm^2 for BF^{LH} and BF^{SH}, respectively, whereas Wickiewicz et al. (42) measured a PCSA of 12.8 cm^2 for the entire biceps femoris muscle. Taken together, these data indicate that the force-generating capacity of the hamstring muscles is greatest for SM and BF^{LH} and smallest for ST and BF^{SH}. Furthermore, the force-generating capacity of SM exceeds that of BF^{LH}. The relative distribution of musculotendon force across the various hamstring muscles calculated in the present study is therefore consistent with what would be expected on the basis of reported PCSA measurements.

The present study was associated with several limitations and assumptions. First, only a single representative trial was analyzed per subject. It is acknowledged that it would have been ideal to have analyzed multiple trials for each subject. However, for a trial to be deemed successful, subjects were required to complete a full stride cycle of valid force plate contacts for the designated lower limb of interest. It typically required several attempts to obtain a representative trial. To avoid the potential confounding effect of fatigue, the study was therefore limited to a single trial per subject. Second, the outputs of the musculoskeletal model are sensitive to the values assumed for the musculotendon force–length–velocity properties. Such properties were not directly measured for

each participant in the present study; rather literature-derived estimates were used (Table 1). However, every effort was made to obtain data that were considered reasonable. For example, pennation angle (α_0) for each individual hamstring muscle matched mean data reported by Ward et al. (41). Furthermore, optimal muscle fiber lengths (l_0^M) for SM, ST, and BF^{LH} were based on data reported by Wickiewicz et al. (42), whereas l_0^M for BF^{SH} was based on data reported by Ward et al. (41). Where it was not possible to source direct measurements of certain hamstrings properties, values were based on recommendations reported by others: data for tendon compliance (ε_0^T) were obtained from Zajac (46), whereas data for tendon slack length (l_s^T) were obtained from Delp et al. (11). It is also worth noting in this regard that the magnitudes of certain musculotendon force–length–velocity properties are far more critical when the relative dynamics within the musculotendon unit is of key interest, i.e., quantifying the dynamics of the tendon versus muscle components. Thelen et al. (39) have previously demonstrated that incremental variations in the value assumed for tendon compliance (ε_0^T in Table 1) substantially influences predictions of BF^{LH} tendon stretch and work done during sprinting. Analyses in the present study were therefore restricted to the quantification of net musculotendon dynamics, which is unfortunate because it is likely that tendon function *in vivo* has an important role in fast movements such as sprinting by storing and releasing energy.

Third, estimates of hamstrings musculotendon force, power, and work done in this study are also limited to the particular method for calculating these parameters. Musculotendon forces were calculated using inverse dynamics–based static optimization. This approach is computationally efficient and has been commonly applied to estimate lower limb muscle forces during locomotion (3,9,16,24,29). However, unlike a dynamic optimization algorithm, static optimization neglects muscle activation dynamics (3). Although it has been shown that static and dynamic optimization algorithms yield similar results when applied to walking (3) and slower speeds of running (29), it is not currently known whether these different computational methods generate consistent results for faster locomotion speeds (i.e., sprinting). The performance criterion used to solve the optimization problem was the sum of the square of muscle activations (3). Although this specific criterion has been applied by previous researchers to compute lower limb muscle forces during sprinting (6,7,33,39), it is acknowledged that minimization of muscle stress during sprinting may not be the most important consideration. Furthermore, such performance criteria may be limited in their capacity to predict cocontraction among antagonistic pairs of muscles (8).

One parameter that would seem to have been somewhat underestimated in this study was peak stance musculotendon force for the biarticular hamstrings. Only BF^{SH} was predicted to be producing force in the second half of stance. As previously mentioned, the magnitude of peak stance hamstrings musculotendon force from the current study is less than that from Chumanov et al. (7). Peak stance hamstrings force ranged from 3.64 $N \cdot kg^{-1}$ for ST to 14.78 $N \cdot kg^{-1}$ for BF^{SH} in this study, whereas it ranged from 6.2 $N \cdot kg^{-1}$ for ST to 12.1 $N \cdot kg^{-1}$ for SM in the study by Chumanov et al. (7) (Table 3). Prior investigations recording lower limb muscle EMG activity during sprinting have found the medial and lateral hamstrings to be active throughout stance (7,21,23, 25,26,35,45). Similarly, EMG activity measured from the medial and lateral hamstrings in this study was found to commence during terminal swing and continue throughout stance until the start of initial swing (Fig. 3, row 5). Although the relationship between EMG and muscle force for fast dynamic contractions is complicated and affected by many factors (12), such experimental data would suggest that, for the biarticular hamstrings during stance, the predicted magnitude of musculotendon force in the present study may be lower than what would be expected.

This inconsistency is most likely attributable to the computational approach used to calculate muscle forces; that is, the inability of inverse dynamics–based static optimization when combined with a minimum-stress performance criterion to adequately predict antagonistic cocontraction. Evidence for this assertion is provided by Collins (8), who evaluated the performance of a variety of optimization algorithms in calculating muscle forces during walking. Although minimization of the sum of muscle activations squared was not specifically tested, optimization algorithms that were included were all found to be particularly insensitive to the prediction of antagonistic quadriceps–hamstrings activity during stance. Predicting high levels of biarticular hamstrings activity throughout stance when there is a net hip flexor moment during the second half of stance and a net knee extensor moment for the majority of stance would not be (from a computational perspective) the most energy-efficient way to distribute the joint moments across the various lower limb muscles. Large muscle forces from the biarticular hamstrings during the first half of stance would likely require greater activations to be computed from the knee extensor muscles, so as to counter the unwanted mechanical effect of the hamstrings at the knee joint and maintain equality with the inverse dynamics–based joint moments. Hence, the hip extensor moment during the first half of stance was preferentially distributed onto the gluteus maximus muscle. In a similar manner, large muscle forces from the biarticular hamstrings during the second half of stance would likely require greater activations to be computed from the hip flexor and knee extensor muscles to maintain equality with the inverse dynamics moments.

Cocontraction of antagonistic muscles can be used to modulate the impedance and thus stability of a joint, which would seem advantageous during the stance phase of sprinting when the lower limb is subjected to a high-frequency impact force. Rather interestingly, it has been demonstrated that people who have learned to cope with compromised knee joint stability (i.e., anterior cruciate ligament deficiency) display increased stance phase hamstrings EMG activity

during locomotion in comparison to a group of healthy counterparts (5). It is therefore speculated that after foot-strike during sprinting, the hamstrings are active not to counter the external moments generated largely by the GRF, but rather to provide alternative functions, such as joint stability and/or proprioception.

Because the biarticular hamstring muscles all reached peak musculotendon strain, produced peak musculotendon force, and performed much negative work during the terminal swing phase of sprinting, it would seem that the hamstrings are likely to be most vulnerable to injury at this time in the stride cycle. Unlike concentric contractions, eccentric contractions have been shown to be capable of producing muscle fiber damage (28). Furthermore, the conclusion that the hamstrings are likely to be at greater risk of injury during terminal swing as opposed to the stance phase concurs with the findings from two recently published, yet independent, case reports that unexpectedly captured biomechanical data of a running athlete suffering a hamstring muscle strain-type injury (18,34). Both of these studies identified terminal swing as the period in the stride cycle when the injury stimulus most likely occurred.

Most hamstring muscle strain injuries involve the biceps femoris muscle (4). It was therefore of interest to determine whether there are biomechanical reasons for this clinical observation; hence parameters such as musculotendon strain, velocity, force, power, and work were compared for each individual hamstring muscle. Based on data from the present study as well as data from previous studies (6,7), the propensity for hamstring muscle strain-type injuries to frequently involve biceps femoris cannot be simply explained on the basis of peak force or the total amount of negative work done because both of these parameters were estimated to be greatest for SM not BF^{LH} or BF^{SH}. In accordance with Thelen et al. (40) and Chumanov et al. (6,7), the amount of musculotendon strain (lengthening with respect to upright stance) was found to distinguish BF^{LH} from SM and ST. An average peak strain of 12.0% was experienced by BF^{LH} during sprinting, which was 2.2% and 3.3% greater than that for SM and ST, respectively (Table 2). These data therefore indicate that the degree of musculotendon strain may be the more relevant parameter in understanding the apparent vulnerability of biceps femoris to injury. This conclusion is consistent with the results from an animal-based study, whereby muscle damage after an eccentric contraction was found not simply to be a function of peak muscle force but rather was due to the magnitude of the strain experienced by the musculotendon unit during contraction (28).

In summary, the present study found the biarticular hamstrings (SM, ST, and BF^{LH}) to be lengthening, producing peak force, and performing much negative work (energy absorption) during the terminal swing phase of the stride cycle. This study also found differing biomechanical loads for each individual hamstring muscle: BF^{LH} exhibited the largest peak strain, ST displayed the greatest lengthening velocity, and SM produced the highest peak force, absorbed and generated the most power, and performed the largest amount of positive and negative work. As peak musculotendon force and strain for BF^{LH}, ST, and SM occurred around the same time during terminal swing, it is suggested that this period in the stride cycle may be when the biarticular hamstrings are at greatest injury risk. On this basis, it is recommended that hamstring injury prevention or rehabilitation programs should be preferentially biased toward strengthening exercises that primarily involve eccentric contractions performed with high loads at longer musculotendon lengths.

Financial support for this project was provided by the Physiotherapy Research Foundation Tagged Sports Physiotherapy Australia research grant (T08-THE/SPA(1)018), the Australian Research Council Discovery Projects grant DP0772838, and the Australian Research Council Linkage Projects grant LP110100262.

The authors thank Doug Rosemond for his assistance with experimental data collection.

The authors have no conflicts of interest to declare.

The results of the present study do not constitute endorsement by the American College of Sports Medicine.

REFERENCES

1. Ae M, Miyashita K, Yokoi T, Hashihara Y. Mechanical power and work done by the muscles of the lower limb during running at different speeds. In: Jonsson B, editor. *Biomechanics X-B*. Champaign (IL): Human Kinetics Publishers, Inc; 1987. p. 895–9.
2. Anderson FC, Pandy MG. Dynamic optimization of human walking. *J Biomech Eng*. 2001;123:381–90.
3. Anderson FC, Pandy MG. Static and dynamic optimization solutions for gait are practically equivalent. *J Biomech*. 2001;34:153–61.
4. Askling CM, Tengvar M, Saartok T, Thorstensson A. Acute first-time hamstring strains during high-speed running. *Am J Sports Med*. 2007;35:197–206.
5. Boerboom AL, Hof AL, Halbertsma JPK, et al. Atypical hamstrings electromyographic activity as a compensatory mechanism in anterior cruciate ligament deficiency. *Knee Surg Sports Traumatol Arthrosc*. 2001;9:211–6.
6. Chumanov ES, Heiderscheit BC, Thelen DG. The effect of speed and influence of individual muscles on hamstring mechanics during the swing phase of sprinting. *J Biomech*. 2007;40:3555–62.
7. Chumanov ES, Heiderscheit BC, Thelen DG. Hamstring musculotendon dynamics during stance and swing phases of high-speed running. *Med Sci Sports Exerc*. 2011;43(3):525–32.
8. Collins JJ. The redundant nature of locomotor optimization laws. *J Biomech*. 1995;28:251–67.
9. Crowninshield RD, Brand RA. A physiologically based criterion of muscle force prediction in locomotion. *J Biomech*. 1981;14:793–801.
10. Delp SL, Anderson FC, Arnold AS, et al. OpenSim: open-source software to create and analyze dynamic simulations of movement. *IEEE Trans Biomed Eng*. 2007;54:1940–50.
11. Delp SL, Loan P, Hoy MG, Zajac FE, Topp EL, Rosen JM. An interactive graphics-based model of the lower extremity to study orthopaedic surgical procedures. *IEEE Trans Biomed Eng*. 1990;37:757–67.
12. Disselhorst-Klug C, Schmitz-Rode T, Rau G. Surface electromyography and muscle force: limits in sEMG–force relationship and new approaches for applications. *Clin Biomech*. 2009;24:225–35.

13. Ekstrand J, Hagglund M, Walden M. Epidemiology of muscle injuries in professional football (soccer). *Am J Sports Med*. 2011; 39:1226–32.
14. Frishberg BA. An analysis of overground and treadmill sprinting. *Med Sci Sports Exerc*. 1983;15(6):478–85.
15. Fuller CW, Laborde F, Leather RJ, Molloy MG. International rugby board rugby world cup 2007 injury surveillance study. *Br J Sports Med*. 2008;42:452–9.
16. Glitsch U, Baumann W. The three-dimensional determination of internal loads in the lower extremity. *J Biomech*. 1997;30:1123–11.
17. Hamner SR, Seth A, Delp SL. Muscle contributions to propulsion and support during running. *J Biomech*. 2010;43:2709–16.
18. Heiderscheit BC, Hoerth DM, Chumanov ES, Swanson SC, Thelen BJ, Thelen DG. Identifying the time of occurrence of a hamstring strain injury during treadmill running: a case study. *Clin Biomech*. 2005;20:1072–8.
19. Heller MO, Bergmann G, Deuretzbacher G, et al. Musculo-skeletal loading conditions at the hip during walking and stair climbing. *J Biomech*. 2001;34:883–93.
20. Hermens HJ, Freriks B, Disselhorst-Klug C, Rau G. Development of recommendations for SEMG sensors and sensor placement procedures. *J Electromyogr Kinesiol*. 2000;10:361–71.
21. Higashihara A, Ono T, Kubota J, Okuwaki T, Fukubayashi T. Functional differences in the activity of the hamstring muscles with increasing running speed. *J Sports Sci*. 2010;28:1085–92.
22. Holzbaur KR, Murray WM, Delp SL. A model of the upper extremity for simulating musculoskeletal surgery and analyzing neuromuscular control. *Ann Biomed Eng*. 2005;33:829–40.
23. Jonhagen S, Ericson MO, Nemeth G, Eriksson E. Amplitude and timing of electromyographic activity during sprinting. *Scand J Med Sci Sports*. 1996;6:15–21.
24. Kim H-J, Fernandez JW, Akbarshahi M, Walter JP, Fregly BJ, Pandy MG. Evaluation of predicted knee joint muscle forces during gait using an instrumented knee implant. *J Orthop Res*. 2009; 27:1326–11.
25. Kyröläinen H, Avela J, Komi PV. Changes in muscle activity with increasing running speed. *J Sports Sci*. 2005;23:1101–9.
26. Kyröläinen H, Komi PV, Belli A. Changes in muscle activity patterns and kinetics with increasing running speed. *J Strength Cond Res*. 1999;13:400–6.
27. Li X, Zhou P, Aruin AS. Taeger–Kaiser energy operation of surface EMG improves muscle activity onset detection. *Ann Biomed Eng*. 2007;35.
28. Lieber RL, Friden J. Muscle damage is not a function of muscle force but active muscle strain. *J Appl Physiol*. 1993;74:520–6.
29. Pandy MG, Andriacchi TP. Muscle and joint function in human locomotion. *Annu Rev Biomed Eng*. 2010;12:401–33.
30. Pedersen DR, Brand RA, Cheng C, Arora JS. Direct comparison of muscle force predictions using linear and non-linear programming. *J Biomech Eng*. 1987;109:192–9.
31. Reinschmidt C, Van Den Bogert AJ, Murphy N, Lundberg A, Nigg BM. Tibiocalcaneal motion during running, measured with external and bone markers. *Clin Biomech*. 1997;12:8–16.
32. Schache AG, Blanch PD, Dorn TW, Brown NAT, Rosemond D, Pandy MG. Effect of running speed on lower limb joint kinetics. *Med Sci Sports Exerc*. 2011;43(7):525–32.
33. Schache AG, Kim H-J, Morgan DL, Pandy MG. Hamstring muscle forces prior to and immediately following an acute sprinting-related muscle strain injury. *Gait Posture*. 2010;32:136–40.
34. Schache AG, Wrigley TV, Baker R, Pandy MG. Biomechanical response to hamstring muscle strain injury. *Gait Posture*. 2009; 29:332–8.
35. Simonsen EB, Thomsen L, Klausen K. Activity of mono- and biarticular leg muscles during sprint running. *Eur J Appl Physiol Occup Physiol*. 1985;54:524–32.
36. Solnik S, Rider P, Steinweg K, Devita P, Hortobagyi T. Taeger–Kaiser energy operator signal conditioning improves EMG onset detection. *Eur J Appl Physiol*. 2010;110:489–98.
37. Stacoff A, Reinschmidt C, Stüssi E. The movement of the heel within a running shoe. *Med Sci Sports Exerc*. 1992;24(6):695–701.
38. Thelen DG, Anderson FC. Using computed muscle control to generate forward dynamic simulations of human walking from experimental data. *J Biomech*. 2006;39:1107–15.
39. Thelen DG, Chumanov ES, Best TM, Swanson SC, Heiderscheit BC. Simulation of biceps femoris musculotendon mechanics during the swing phase of sprinting. *Med Sci Sports Exerc*. 2005; 37(11):1911–8.
40. Thelen DG, Chumanov ES, Hoerth DM, et al. Hamstring muscle kinematics during treadmill sprinting. *Med Sci Sports Exerc*. 2005; 37(1):108–14.
41. Ward SR, Eng CM, Smallwood LH, Lieber RL. Are current measurements of lower extremity muscle architecture accurate? *Clin Orthop Rel Res*. 2009;467:1074–82.
42. Wickiewicz TL, Roy RR, Powell PL, Edgerton VR. Muscle architecture of the human lower limb. *Clin Orthop Rel Res*. 1983; 179:275–83.
43. Wood GA. Biomechanical limitations to sprint running. In: Van Gheluwe B, Atha J, editors. *Current Research in Sports Biomechanics*. Basel (Switzerland): Karger; 1987. p. 58–71.
44. Yamaguchi GT, Zajac FE. A planar model of the knee joint to characterise the knee extensor mechanism. *J Biomech*. 1989;22: 1–10.
45. Yu B, Queen RM, Abbey AN, Liu Y, Moorman CT, Garrett WE. Hamstring muscle kinematics and activation during overground sprinting. *J Biomech*. 2008;41:3121–6.
46. Zajac FE. Muscle and tendon: properties, models, scaling, and application to biomechanics and motor control. In: Bourne JR, editor. *CRC Critical Reviews in Biomedical Engineering*. Baca Raton (FL): CRC Press; 1989. p. 359–411.
47. Zajac FE. Muscle coordination of movement: a perspective. *J Biomech*. 1993;26:109–24.